NEUTRON-RICH LIGHT-NUCLEI STUDIED VIA REACTIONS WITH THE ^{9}Li BEAM*

M. Sigmund [a], N. Soić [a], M. Alcorta Moreno [b], J. Bishop [c], A.D. Brooks [c], L.E. Charón García [b], T. Davinson [d], A. Di Pietro [e], D. Dell'Aquila [f,g], F. Falezza [c], M. Freer [c], I. Gašparić [a], D. Jelavić Malenica [a], T. Kokalova Wheldon [c], M. La Cognata [e], A. Lennarz [b], I. Lihtar [a], I. Martel Bravo [h], M. Milin [i], C. Müller-Gatermann [j], S. Murillo Morales [b], L. Palada [a], C. Parker [k], S.H. Pirrie [c], L. Redigolo [l], B. Reed [b,m], M. Sferazza [n], R. Smith [o], A. Teigelhoefer [b], O. Tindle [o], N. Vukman [a,p,q]

[a]Ruđer Bošković Institute, Zagreb, Croatia
[b]TRIUMF, Vancouver, BC, Canada
[c]University of Birmingham, Birmingham, UK
[d]University of Edinburgh, Edinburgh, UK
[e]INFN-LNS, Catania, Italy
[f]INFN — Sezione di Napoli, Naples, Italy
[g]Università degli Studi di Napoli "Federico II", Naples, Italy
[h]University of Huelva, Huelva, Spain
[i]University of Zagreb, Zagreb, Croatia
[j]Argonne National Laboratory, Lemont, IL, USA
[k]Ohio University, Athens, OH, USA
[l]University of Catania, Catania, Italy
[m]St. Mary's University, Halifax, Nova Scotia, Canada
[n]Université Libre de Bruxelles, Bruxelles, Belgium
[o]Sheffield Hallam University, Sheffield, UK
[p]INFN — Sezione di Perugia, Perugia, Italy
[q]University of Split, Split, Croatia

Received 10 November 2025, accepted 15 January 2026, published online 31 March 2026

The structure of light nuclei is a particularly active area of research due to their small number of nucleons and yet a large variety of nuclear structure phenomena. In this contribution, preliminary results on ^{9}Li and ^{10}Be states, some of which indicate their pronounced clustered structure, are discussed.

DOI:10.5506/APhysPolBSupp.19.1-A11

* Presented at the XXXVIII Mazurian Lakes Conference on Physics, Piaski, Poland, August 31–September 6, 2025.

1. Introduction

The structure of light nuclei has played a crucial role in understanding the behavior of the nuclear force in few-body systems and the fundamental principles of nucleosynthesis in stars. Due to the small number of nucleons and the wide variety of phenomena they exhibit, light nuclei continue to be an active area of both theoretical and experimental research.

Among many phenomena observed in light nuclei, clustering has been a subject of interest since the earliest days of nuclear physics and the discovery of radioactivity. Clustering is the tendency of nucleons to group themselves into smaller, more strongly bound substructures, known as clusters. It is most pronounced in α-conjugate nuclei, since the α particle is extremely well bound, compact, and is a boson, making the formation of such α-clustered configurations energetically more favorable around the α-decay threshold. The well-known examples are the nucleus of ^{8}Be and the Hoyle state in ^{12}C.

Even from the earliest times, adding and removing nucleons from an α-conjugate nucleus has been of interest to many nuclear structure studies [1]. In neutron-rich nuclei, a phenomenon named "nuclear molecules" has been the topic of many theoretical and experimental studies throughout the years. In such nuclei, extra neutrons fill up molecular orbitals between the clusters, similar to those in atomic molecules, hence the term.

The description of cluster structures has been tackled with a wide variety of theoretical approaches, including empirical cluster models, phenomenological, and *ab initio* models [2–4]. The mentioned comprehensive reviews summarize recent developments in understanding the structures in light nuclei and highlight the importance of the clustering phenomena and their impact on nuclear structure, reaction dynamics, and nuclear astrophysics. They also emphasize the coexistence of cluster and shell-model features in neutron-rich isotopes and discuss the challenges in fully understanding the underlying mechanisms.

The pivotal examples of nuclear molecules are the nuclei of ^{9}Be and ^{10}Be. When an extra neutron is added to the unbound nucleus of ^{8}Be, it becomes stable and exhibits a perfect example of the nuclear molecule [5]. Recently, ^{10}Be has been probed and proven to exhibit molecular structure even in the ground state, in nice agreement with Tohsaki–Horiuchi–Schuck–Röpke (THSR) and Antisymmetrized Molecular Dynamics (AMD) calculations [6]. That is in alignment with recent theoretical *ab initio* results from Nuclear Lattice Effective Field Theory [7], where by identifying clusters and valence neutrons, nuclear molecular orbitals emerge naturally in the p-shell beryllium isotopes.

Unlike ^{10}Be, the ^{9}Li structure has not yet been extensively studied. Interestingly enough, ^{9}Li has the smallest charge radius [8] in the chain of Li isotopes, indicating that it is the least deformed. In later research [9],

spectroscopic factors of the ground and first few excited states in ^{9}Li have been reported. Spectroscopic factors of the ground state indicate that it is, to a large extent, constructed as ^{8}Li+n, making it a compact core for the halo nucleus ^{11}Li. Still, an open question remains, whether the t+α cluster structure is preserved [10–12]. Recently, it was reported that the ^{9}Li cluster structure emerges at higher excitation energies, around 2 MeV above the ^{6}He+t decay threshold [13].

In 2023 and 2024, an experiment with the aim of studying exotic structures in carbon isotopes was conducted. The experiment used a neutron-rich ^{9}Li rare isotope beam on a natural boron target. In the aforementioned collisions, many neutron-rich nuclei are produced, and here some preliminary results on ^{10}Be as well as on ^{9}Li states will be presented.

2. Experimental setup

The experiment exploited a ^{9}Li beam at 8.31 MeV/u with a natural boron target (1000 μg/cm^2) on aluminum backing (900 μg/cm^2). It is important to mention that the natural boron target consists of approximately 80% ^{11}B and 20% ^{10}B. The experiment was conducted at the TUDA chamber of the ISAC-II facility at TRIUMF, Canada [14].

As an experimental setup, 6 silicon detector telescopes were used (50 μm or 20 μm+1000 μm Micron Semiconductor Silicon Strip Detectors), 4 of which were at more forward angles, and 2 at more backward angles. Details of the experimental setup, calibration, and identification algorithm can be found in [15].

3. Results

3.1. Particle identification plot

Detector telescopes were used to have proper particle identification. Namely, the particle deposits some of its energy when passing through the first stage of detection (ΔE detector), and, finally, the remaining energy is deposited in the second stage of detection, where the particle stops. The relations between those energies depend on the particles' Z, A, and kinetic energy according to the Bethe–Bloch formula. It gives us an identification plot as seen on the left-hand side of Fig. 1. In the figure, only data from one strip of one of the forward detectors, covering a relatively narrow θ angle range, is shown.

On the identification plot, distinct groups of events corresponding to the detected elements (H, He, Li, Be, and B, from bottom to top) can be clearly observed. Within each group, less separated loci of events indicate the different isotopes, since the energy deposition depends more strongly on the nuclear charge than on the nuclear mass.

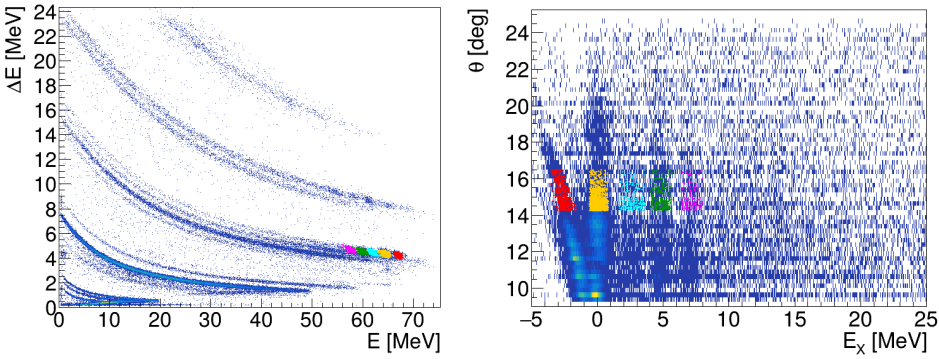

Fig. 1. (Color online) Identification plot for one strip of forward detector telescope with marked sets of events corresponding to different scattering processes (left) — elastic scattering of ^{9}Li on Al (red, the most right pile of events), ^{9}Li on ^{11}B (yellow, the second most right pile), and inelastic scattering of ^{9}Li on ^{11}B (cyan, green, and magenta). The detecting angle (θ) of ^{9}Li *versus* the excitation energies reconstructed in the whole detector telescope, assuming that ^{9}Li was scattered off ^{11}B (right).

In the experiment, the ^{9}Li beam was scattered off the B target with an Al backing. Elastic and inelastic events are marked in Fig. 1. In the ΔE–E histogram, data from a small range of θ angles is presented and marked groups of events are separated. Due to the kinematics of scattering, outgoing ^{9}Li has different kinetic energy depending on what was the scattering target and whether the scattering was elastic or inelastic.

For all events with detected ^{9}Li, its excitation energy after the scattering was calculated assuming scattering off an ^{11}B target using the missing mass method. On the right panel of Fig. 1, the scattering angle of ^{9}Li in the laboratory frame of reference is plotted *versus* the reconstructed excitation energy. From the collected data, it is not possible to identify which nuclei in the exit channel are in the excited states, target-like, projectile-like or both at the same time.

The loci of events that form a straight line are events in which ^{9}Li was scattered off ^{11}B, since the correct scattering target is assumed, while the loci of events when scattering happened on Al are curved, as seen in the left part of the plot. From the plots in Fig. 1, it can be easily understood which marked group of events corresponds to which marked excitation event. Since the ΔE–E plot shows events only from one strip and the right plot shows events from the whole detector telescope, only events in that angular area of the chosen strip are marked.

3.2. ^{9}Li inclusive excitation energy spectrum

In the inclusive excitation energy spectrum of detected ^{9}Li events (Fig. 2, left), 5 peaks are visible. The leftmost peak originates from the events of ^{9}Li nuclei elastically scattered off Al. Typically, this peak is broad and poorly defined. However, its current Gaussian-like shape is a consequence of the ^{9}Li elastic scattering cross section. As seen in Fig. 1 right, most of the detected events are at more forward laboratory-frame angles. Furthermore, the detected energy slowly changes with the angle of detection, resulting in a Gaussian-like projected curve with an asymmetrical tail on the left.

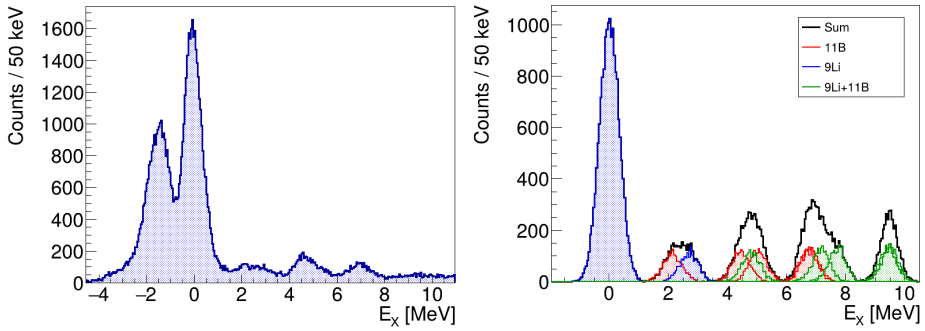

Fig. 2. (Color online) Inclusive excitation energy spectrum for events when ^{9}Li is detected, experimental data (left) and Monte-Carlo simulated data of ^{9}Li scattering off ^{11}B target data (right). Simulated are events of elastic scattering and the first excited state of ^{9}Li (blue, around 0 MeV and 2.7 MeV), excited states of ^{11}B (red, around 2.1 MeV, 4.4 MeV, 5 MeV, 6.7 MeV), and events when simultaneously ^{9}Li and ^{11}B are in the excited states (green). Black is the summed curve of all the mentioned contributions.

The most populated peak is due to the elastic scattering of ^{9}Li off ^{11}B. The peak width comes mostly from the uncertainty of the energy deposited in the target ($\sigma_{\text{target}} \approx 200$ keV), intrinsic detector resolution (≈ 1 %), and position/angular resolution ($\approx 1^{\circ}$). Those effects were taken into account when ^{9}Li scattering off ^{11}B target was simulated (Fig. 2, right), using the UNISim-tool [16] framework. The Monte-Carlo simulations included elastic scattering off ^{11}B, inelastic scattering to the first excited state of ^{9}Li (blue), inelastic scattering to the first four excited states in ^{11}B (red), as well as inelastic scattering with simultaneous excitations of ^{9}Li and ^{11}B (green). Only the contribution of the first excited state in ^{9}Li is simulated, since other excited states are not particle stable and cannot contribute to this inclusive spectrum. Simulated spectra are not scaled, but they still nicely illustrate the contributions to the remaining peaks in the inclusive spectrum.

The peak around 2 MeV has two possible contributions, the first excited state of ^{11}B and the first excited state of ^{9}Li. The next peak, around 5 MeV, comes from two possible excitations of ^{11}B, or when both ^{9}Li and ^{11}B are in the first excited state. Similar is for the rest of the peaks. Scattering off ^{10}B produces smeared background in the spectrum.

3.3. ^{10}Be inclusive excitation energy spectrum

Similarly, when ^{10}Be is detected, an inclusive excitation energy spectrum is made using the missing mass method, as shown in Fig. 3. That spectrum represents all possible excited states in the assumed reaction ^{11}B(^{9}Li,^{10} Be)^{10}Be. On the spectrum, a barely visible ground-state peak can be spotted, at higher energies, a peak between 3 MeV and 4 MeV is seen due to the first excited state of ^{10}Be. The next peak contains four possible excited states of ^{10}Be around 6 MeV and also states around 7 MeV, together with the sum of the first excited states in both ^{10}Be nuclei. The peak around 10 MeV originates from the ^{10}Be state around 9.6 MeV together with 10.6 MeV state of ^{10}Be producing the asymmetry at the right side of the peak, as well as the sum of the first excited state in one ^{10}Be nucleus and some of the states around 6 MeV in the second ^{10}Be nucleus.

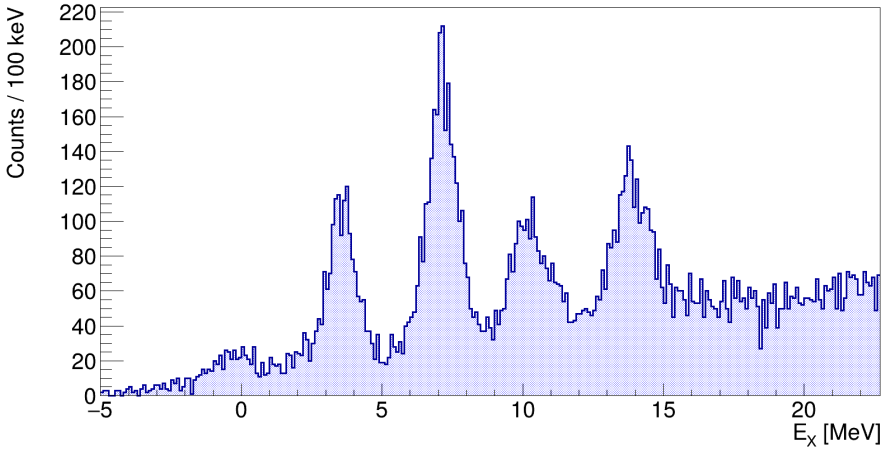

Fig. 3. Inclusive excitation energy spectrum for events of detected ^{10}Be.

3.4. The ^{10}Be states with cluster structure

As mentioned in Section 2, the target was composed of natural boron, meaning it contains both ^{10}B ($\approx$ 20 %) and ^{11}B. To separate the events of the reactions happening on two different target constituents, a useful

tool in the analysis of the coincidence data from the kinematically complete measurements is the Catania plot [17]. In that plot, the events originating from different reactions are assembled around the lines with $-Q$ value as the y-intercept and A^{-1} of the undetected nucleus as the slope. On the left panel of Fig. 4, is presented the ^{6}He+^{4}He coincidence with the lines corresponding to the reactions $^{10/11}$B(^{9}Li,^{6} He^{4}He)$^{9/10}$Be. The events originating from the reaction of the ^{10}B with the ^{9}Be in the ground state and the excited state (magenta lines) are separated from the events corresponding to the ^{10}Be states (green lines). By selecting only the events corresponding to the ^{10}Be states, the background contributions from the reactions on the ^{10}B are excluded from further data analysis. Applying the invariant mass technique on the selected ^{6}He+^{4}He coincidence events, the ^{10}Be excitation energy spectrum presented on the right of Fig. 4 was constructed.

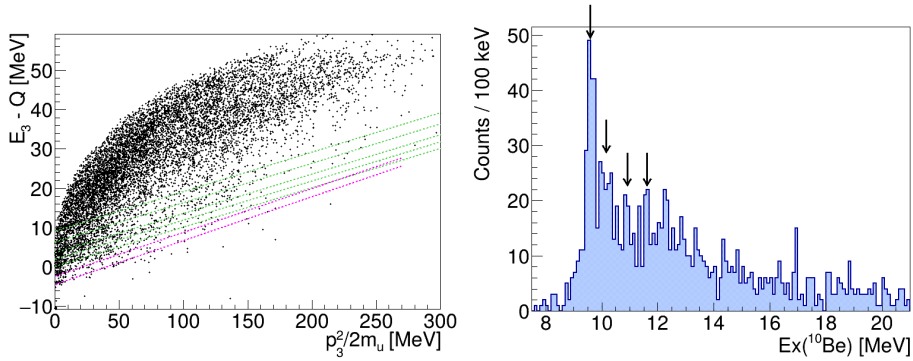

Fig. 4. (Color online) The Catania plot for ^{6}He+^{4}He coincidence events (left); green (upper) lines indicate the ^{10}Be states, magenta (lower) lines the ^{9}Be states; ^{10}Be excitation energy spectrum for the ^{6}He+^{4}He coincidence events (right).

The most populated state in the spectrum is the one around 9.6 MeV, which has been observed to decay via both ^{9}Be+n and ^{6}He+^{4}He channels [18]. That implies the state has a complex structure, featuring both single-particle and cluster configurations. Its strong population in the experiment is in agreement with the available results on the ^{10}Be spectroscopy.

The next populated state is around 10.2 MeV, located on the high-energy side of the strong 9.6 MeV peak, and with smaller statistics. Existing experimental results confirm its pronounced cluster structure and fit with its proposed molecular structure [2].

There are indications for the peak around 10.9 MeV which would correspond to the state at 10.6 MeV, known to decay into ^{9}Be$+n$ and ^{6}He$+^{4}$He.

Another indication for the peak is around 11.6 MeV, most likely corresponding to the state at 11.8 MeV, but contribution from 11.2 MeV state cannot be excluded. Both states decay via α.

4. Conclusion

An experiment using a radioactive ^{9}Li beam on a natural boron target (with Al backing) was performed and previously reported states in neutron-rich nuclei have been observed. Some of the preliminary results of the limited data set have been presented here. The thick target increased production yield but limited the energy resolution, requiring detailed Monte-Carlo simulations for interpretation. These preliminary findings on a limited data set encourage the expectation that analyzing the complete data set will yield new insights into the nuclear structure of ^{9}Li and ^{10}Be.

This work was supported in part by the HrZZ project No. IP-2018-01-1257, NextGenerationEU: MZ3-25, 01-986/1-2025 project, and by the U.S. DoE, Office of Nuclear Physics, award No. DE-AC02-06CH11357.

REFERENCES

[1] L.R. Hafstad *et al.*, *Phys. Rev.* **54**, 681 (1938).
[2] W. von Oertzen *et al.*, *Phys. Rep.* **432**, 43 (2006).
[3] M. Freer *et al.*, *Rev. Mod. Phys.* **90**, 035004 (2018).
[4] I. Lombardo *et al.*, *Riv. Nuovo Cimento* **46**, 521 (2023).
[5] P. Descouvemont, *Nucl. Phys. A* **699**, 463 (2002).
[6] P.J. Li *et al.*, *Phys. Rev. Lett.* **131**, 212501 (2023).
[7] S. Shen *et al.*, *Phys. Rev. Lett.* **134**, 162503 (2025).
[8] R. Sánchez *et al.*, *Phys. Rev. Lett.* **96**, 033002 (2006).
[9] R. Kanungo *et al.*, *Phys. Lett. B* **660**, 26 (2008).
[10] F. Kobayashi *et al.*, *Phys. Rev. C* **89**, 024315 (2014).
[11] Y. Kanada-En'yo *et al.*, *Phys. Rev. C* **85**, 024303 (2012).
[12] H.T. Fortune, *Eur. Phys. J. A* **54**, 51 (2018).
[13] W.H. Ma *et al.*, *Phys. Rev. C* **103**, L061302 (2021).
[14] G.C. Ball *et al.*, *J. Phys. G: Nucl. Part. Phys.* **38**, 024003 (2011).
[15] M. Sigmund *et al.*, *EPJ Web Conf.* **311**, 00026 (2024).
[16] D. Dell'Aquila, `https://github.com/dellaquilamaster/UNISim-tool`
[17] E. Costanzo *et al.*, *Nucl. Instrum. Methods Phys. Res. A* **295**, 373 (1990).
[18] N. Soić *et al.*, *Europhys. Lett.* **34**, 7 (1996).